Acta Crystallographica Section B
Structural Science
ISSN 0108-7681

Unravelling the chemical basis of the bathochromic shift in the lobster carapace; new crystal structures of unbound astaxanthin, canthaxanthin and zeaxanthin

Giuditta Bartalucci,[a] Jennifer Coppin,[a] Stuart Fisher,[a] Gillian Hall,[a] John R. Helliwell,[a] Madeleine Helliwell[a]* and Synnøve Liaaen-Jensen[b]

[a]Department of Chemistry, University of Manchester, Manchester M13 9PL, England, and [b]Department of Chemistry, Norwegian University of Science and Technology, Trondheim, Norway

Correspondence e-mail: madeleine.helliwell@manchester.ac.uk

Received 5 October 2006
Accepted 5 December 2006

The crystal structures of the unbound carotenoids, synthetic astaxanthin (3*S*,3′*S*:3*R*,3′*S*:3*R*,3′*R* in a 1:2:1 ratio), canthaxanthin and (3*R*,3′*S*, *meso*)-zeaxanthin are compared with each other and the protein bound astaxanthin molecule in the carotenoprotein, β-crustacyanin. Three new crystal forms of astaxanthin have been obtained, using different crystallization conditions, comprising a chloroform solvate, a pyridine solvate and an unsolvated form. In each structure, the astaxanthin molecules, which are similar to one another, are centrosymmetric and adopt the 6-s-*cis* conformation; the end rings are bent out of the plane of the polyene chain by angles of −42.6 (5), −48.9 (5) and −50.4 (3)°, respectively, and are disordered, showing the presence of both *R* and *S* configurations (in a 1:1 ratio). In the crystal packing of the chloroform and pyridine solvates, the astaxanthin molecules show pair-wise end-to-end intermolecular hydrogen bonding of the adjacent 3-hydroxyl and 4-keto oxygens, whereas in the unsolvated crystal form, the hydrogen-bonding interaction is intermolecular. In addition, there are intermolecular C—H hydrogen bonds in all three structures. The canthaxanthin structure, measured at 100 and 293 K, also adopts the 6-s-*cis* conformation, but with disorder of one end ring only. The rotation of the end rings out of the plane of the polyene chains (*ca* −50 ° for each structure) is similar to that of astaxanthin. A number of possible C—H hydrogen bonds to the keto O atoms are also observed. (3*R*,3′*S*, *meso*)-zeaxanthin is centrosymmetric with a C5—C6—C7—C8 torsion angle of −74.9 (3)°; the molecules show pair-wise hydrogen bonding between the hydroxyl O atoms. In addition, for all the crystal structures the polyene chains were arranged one above the other, with intermolecular distances of 3.61–3.79 Å, indicating the presence of π-stacking interactions. Overall, these six crystal structures provide an ensemble of experimentally derived results that allow several key parameters, thought to influence colour tuning of the bathochromic shift of astaxanthin in crustacyanin, to be varied. The fact that the colour of each of the six crystals remains red, rather than turning blue, is therefore especially significant.

1. Introduction

Astaxanthin (3,3′-dihydroxy-β,β-carotene-4,4′-dione), AXT, shown schematically in Figs. 1(*a*)–(*c*), is a carotenoid occurring in nature as three optical isomers [3*S*,3′*S*, 3*R*,3′*S*, *meso* and 3*R*,3′*R* (*SS*, *RS* and *RR*) in various ratios; Rønneberg *et al.*, 1980; Renstrøm *et al.*, 1982]. It is present in shrimps, crabs and lobsters, as well as in many invertebrate animals, where interaction with a protein can cause the astaxanthin molecule to change its colour from an orange/red colour in the unbound form to a deep slate blue/black. In the lobster shell, the protein

α-crustacyanin, which consists of an assembly of sixteen 20 kDa apoproteins and 16 bound astaxanthin molecules, is known to be responsible for this blue/black colour of the live lobster (Cianci *et al.*, 2002; Chayen *et al.*, 2003; Zagalsky, 2003). Denaturing of this protein by boiling of the lobster gives the familiar bright red colour of cooked lobster. There has been much interest in the cause of this hypsochromic shift, spanning over 100 years (Newbiggin, 1897; Wald, 1948), and determination of the crystal structure of β-crustacyanin (β-CR) in 2002 to 3.2 Å resolution allowed many questions about the bound astaxanthin molecules to be answered (Cianci *et al.*, 2002). β-Crustacyanin is a dissociation product of α-crustacyanin and is a heterodimer consisting of two apo protein monomers (gene types I and II) with two astaxanthin molecules, which bind to the protein by straddling each subunit. Both astaxanthin molecules have similar, but not identical, protein environments and display essentially identical conformations. At one end of each astaxanthin, the 4-keto group is linked to a bound water molecule by a hydrogen bond; the evidence for these two water molecules required corroboration from an earlier high-resolution crystal structure of the A1 protein (Cianci *et al.*, 2001), and an investigation of electron-density map properties at 3.2 Å resolution (Minichino *et al.*, 2003). The other end of each astaxanthin is connected to the neighbouring subunit with their C4-keto groups each within hydrogen-bonding distance of a His residue. A substantial conformational change of the astaxanthin molecule was found to occur on binding to the protein, with the molecules both in the 6-s-*trans* conformation, the end-ring approximately coplanar with the polyene chains and a significant bowing of the polyene compared with that found in the structure of canthaxanthin (β,β-carotene-4, 4′-dione; see Fig. 1*d*), which was used as a model for unbound astaxanthin, in the absence of a crystal structure of unbound astaxanthin at the time. Theories that have been put forward as to the cause to the bathochromic shift include the following:

(i) the coplanarization of the β-end rings with the polyene chain increases the conjugation in the planar chromophoric system;

(ii) the bowing of the astaxanthin molecule relieves the strain in the planar, 6-s-*trans* configuration of the protein bound AXT molecule;

(iii) a generally hydrophobic environment, where dissolution in different solvents provokes different bathochromic shifts (Britton, 1995);

(iv) an electronic polarization effect stems from hydrogen bonding of histidine, and/or water, with the bound astaxanthins;

(v) an exciton interaction arises from the close proximity of the two bound astaxanthins; the closest distance is ~ 7 Å and the two chains are inclined at an angle of 120°.

It is now generally accepted that the coplanarization of the end rings accounts for up to a third of the overall bathochromic shift of the absorption maximum from 472 nm in unbound astaxanthin dissolved in hexane to 580 nm in the β-CR molecule (Durbeej & Eriksson, 2003, 2004; van Wijk *et al.*, 2005; Ilagan *et al.*, 2005). In the unbound molecule there is already some partial conjugation of the polyene chain with the end rings (Durbeej & Eriksson, 2004) and the coplanarization has the effect of extending this to 13 conjugated double bonds. Even in the recent literature, there is still disagreement as to how the additional bathochromic shift arises; Weesie *et al.* (1997) proposed that protonation of the C4 keto groups is responsible for the polarization of the chromophore, thus reducing the energy difference between the HOMO and LUMO orbitals. More recently, Durbeej & Eriksson (2003, 2004) put forward the theory that the polarization effect is caused by hydrogen bonding of the C4 keto group, particularly to the His residue, which they suggested must be protonated. In 2005, Lugtenburg and co-workers (van Wijk *et al.*, 2005) dismissed the polarization theory as a major contribution to the spectral shift, citing evidence from ^{13}C NMR spectroscopy studies, and instead proposed that the approach of the chromophores to within 7 Å of one another at 120° inclination gives rise to an exciton interaction, leading to the observed spectral shift. The calculations were performed assuming a vacuum environment (*i.e.* with a dielectric constant of 1.0), but the crystal structure of β-CR (Cianci *et al.*, 2002) shows that an unidentified molecule sits between the two AXT molecules at the closest approach, which would, *via* the dielectric constant, weaken the exciton effect. The further shift in the absorption in the α-CR to that seen in the β-CR was proposed to arise from increased exciton coupling caused by additional aggregation of astaxanthin molecules. Ilagan *et al.* (2005), explaining

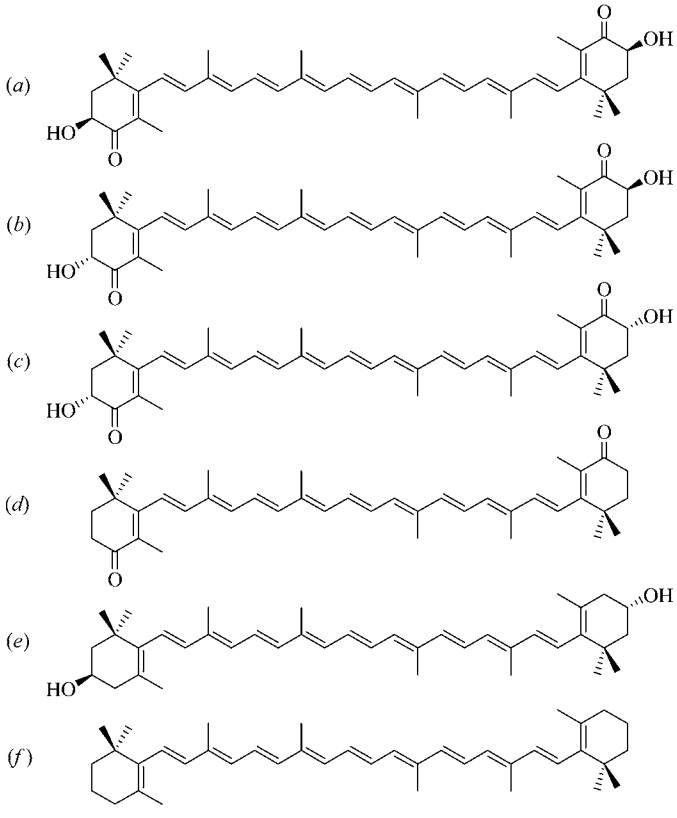

Figure 1
Scheme of (*a*) *SS*-astaxanthin, (*b*) *RS*-astaxanthin, (*c*) *RR*-astaxanthin, (*d*) canthaxanthin, (*e*) *RS*-zeaxanthin and (*f*) β-carotene.

the femtosecond time-resolved absorption spectroscopy of AXT in solution and in β-CR, supported the idea that dimerization of AXT in crustacyanin is the primary molecular basis of the bathochromic shift. The bowing of the astaxanthin molecule in the bound form was considered to have a negligible effect on the absorption (Durbeej & Eriksson, 2004). These theories have been reviewed recently in Durbeej & Eriksson (2006)

In order to investigate these colour-tuning parameters further, we have successfully crystallized and determined the crystal structures of three crystal forms of astaxanthin and one each of canthaxanthin and *RS*-zeaxanthin [(3*R*,3′*S*,*meso*)-β,β-carotene-3,3′-diol; Fig. 1]. This has provided us with an ensemble of related crystal structures, as well as much more precise structural information regarding the interactions of the end rings and packing of the molecules than the β-CR structure at 3.2 Å resolution could offer. The unsolvated crystal form of astaxanthin, which we report here, has been described previously by Hashimoto *et al.* (2002), but the atom coordinates were not deposited in the CSD (Cambridge Structural Database), and in any case our results are more precise (see later). The crystal structure of canthaxanthin has also been reported by Bart & MacGillavry (1968), but again our new crystal structure is more precise due to the use of modern crystallographic apparatus, as well as sample cryocooling. We also report the room-temperature crystal structure of canthaxanthin, to compare directly with the Bart & MacGillavry (1968) room-temperature structure. The crystal structure of the bis[menthyl carbonate] derivative of *RR*-zeaxanthin has been reported previously (Linden *et al.*, 2004), but to our knowledge the crystal structure of *RS*-zeaxanthin reported here is the first crystal structure of a free zeaxanthin. We will show that important variations of the various proposed colour-tuning parameters have been achieved in a field where it was previously regarded as notoriously difficult to produce crystals. Also, two room-temperature crystal structures are reported, introducing temperature as an additional variable which could be investigated; this was not possible in the β-CR studies, where cryocooling was essential (Cianci *et al.*, 2002).

2. Experimental

2.1. Methods of crystallization

The carotenoids used were synthetic samples originating from Hoffmann-La Roche, Basel. A 1:2:1 mixture of the three optical isomers of astaxanthin (*SS*, *RS* and *RR*; Bernhard, 1989) was employed for crystallization; the synthon for AXT containing the hydroxy group is optically inactive and consists of the *R* and *S* form in equal amounts. By statistical probability when two such end groups are added to the same molecule the result is 1:2:1 for the *SS*, *RS* and *RR* isomers; the composition of synthetic AXT is determined by HPLC of diesters of (−)-camphanic acid (Vecchi & Müller, 1979). Synthetic *RS*-zeaxanthin (Rüttimann & Mayer, 1980) and commercial canthaxanthin were used. In each case, vapour diffusion methods were used to grow suitable crystals. For the chloroform solvate of AXT (AXT-Cl), acicular crystals were obtained from chloroform/hexane. The pyridine solvate, AXT-py and unsolvated, AXT-un, crystals of AXT were obtained as platy crystals from pyridine/hexane. However, much larger platy crystals of the unsolvated form were subsequently obtained from pyridine/water, and a crystal obtained by this method was used in the crystal structure determination described here. Large platy crystals of canthaxanthin were grown from dichoromethane/hexane and acicular crystals of *RS*-zeaxanthin were crystallized from pyridine/water.

2.2. Data collection and refinement of the structures

Data were collected in each case using a Bruker APEX CCD diffractometer (Bruker, 2001) using Mo $K\alpha$ radiation; data processing was carried out using *SAINT* (Bruker, 2002). Absorption corrections were not applied, except in the case of *RS*-zeaxanthin, where a semi-empirical absorption correction was applied using *SADABS* (Bruker, 2001). Cryocooling to 100 K, using an Oxford Cryosystems Cryostream 700 open-flow cryostat (Cosier & Glazer, 1986), was carried out for all samples except the unsolvated crystal form of astaxanthin, since the crystal broke up at low temperature. An additional room-temperature crystal structure of canthaxanthin was also determined from the same crystal used in the low-temperature study for comparison with the previous results (Bart & MacGillavry, 1968). The structures were solved by direct methods and H atoms were included in calculated positions using the riding method, except for the O—H H atoms in AXT-Cl and AXT-py. In each AXT structure, some disorder of the end rings was found; the occupancies of the disordered components were constrained to sum to unity and the ratio of the different conformations was found to be *ca* 50:50, consistent with the 1:2:1 ratio of *RR*, *RS* and *SS* isomers. For AXT-Cl, two restraints were applied to the geometry of the O—H group. For the pyridine solvate, AXT-py, the pyridine molecule was poorly ordered and it is possible that the nitrogen position was not ordered at one position; the H atoms were not visible on a difference map, so the N-atom position was selected as that which gave the lowest displacement parameter when all the atoms of the ring were defined as carbon. Restraints were applied to the bond lengths of the pyridine molecule and the O—H group of the AXT molecule. Also, because the crystal was rather weakly diffracting, the data were cut at 0.9 Å resolution for this sample. For AXT-un, the O—H hydrogen was included in a calculated position so as to form the best hydrogen bond to O4. The canthaxanthin structures at 100 and 293 K showed disorder of one end-ring only, which was treated as for the AXT crystal structures; the occupancies of the major disorder components refined to values of 0.610 (3) and 0.682 (9) for the canthaxathin structures measured at 100 and 293 K, respectively. The *RS*-zeaxanthin structure did not show any disorder of the end rings, but contained a number of disordered solvent atoms, which were assumed to be partially occupied water molecules. *SQUEEZE* (van der Sluis & Spek, 1990) was used to account for the disordered solvent, determining an electron count of

Table 1
Experimental details.

	Chloroform solvate of AXT	Pyridine solvate of AXT	Unsolvated AXT	Canthaxanthin at 100 K	Canthaxanthin at 293 K	*RS*-Zeaxanthin
Crystal data						
Chemical formula	$C_{40}H_{52}O_4\cdot 2CHCl_3$	$C_{40}H_{52}O_4\cdot 2C_5H_5N$	$C_{40}H_{52}O_4$	$C_{40}\ H_{52}O_2$	$C_{40}\ H_{52}O_2$	$C_{40}\ H_{56}O_2\cdot 3H_2O$
M_r	835.55	755.02	596.82	564.82	564.82	622.90
Cell setting, space group	Triclinic, $P\overline{1}$	Monoclinic, $P2_1/n$	Triclinic, $P\overline{1}$	Triclinic, $P\overline{1}$	Triclinic, $P\overline{1}$	Monoclinic, $C2/c$
Temperature (K)	100 (2)	100 (2)	293 (2)	100 (2)	293 (2)	100 (2)
a, b, c (Å)	5.9588 (8), 11.8583 (16), 15.647 (2)	18.568 (4), 6.1926 (13), 19.803 (4)	8.5371 (10), 8.6632 (11), 13.2984 (16)	8.5068 (9), 14.2208 (16), 15.5262 (17)	8.5919 (11), 14.3168 (18), 15.9405 (19)	49.670 (15), 13.181 (4), 6.0588 (19)
α, β, γ (°)	79.036 (2), 80.499 (3), 82.506 (2)	90, 107.746 (4), 90	95.145 (2), 107.409 (2), 98.765 (2)	105.870 (2), 95.227 (2), 106.512 (2)	105.569 (2), 96.118 (3), 107.024 (2)	90, 94.425 (6), 90
V (Å^3)	1065.0 (3)	2168.7 (8)	917.93 (19)	1702.9 (3)	1769.2 (4)	3955 (2)
Z	1	2	1	2	2	4
D_x (Mg m^{-3})	1.303	1.156	1.080	1.102	1.060	1.046
Radiation type	Mo $K\alpha$	Mo $K\alpha$	Mo $K\alpha$	Mo $K\alpha$	Mo $K\alpha$	Mo $K\alpha$
Absorption coefficient (mm^{-1})	0.443	0.072	0.068	0.065	0.063	0.067
Crystal form, colour	Needle, red	Plate, red	Plate, red	Block, dark red	Block, dark red	Plate, orange
Crystal size (mm)	0.65 × 0.05 × 0.02	0.60 × 0.15 × 0.05	0.60 × 0.30 × 0.05	0.50 × 0.35 × 0.30	0.50 × 0.35 × 0.30	0.90 × 0.15 × 0.05
Data collection						
Diffractometer	CCD area detector	CCD area detector	CCD area detector	CCD area detector	CCD area detector	CCD area detector
Data collection method	φ and ω scans	φ and ω scans	φ and ω scans	φ and ω scans	φ and ω scans	φ and ω scans
Absorption correction	None	None	None	None	None	Multi-scan (based ion symmetry-related measurements)
T_{min}	–	–	–	–	–	0.807
T_{max}	–	–	–	–	–	1.000
No. of measured, independent and observed reflections	7182, 3634, 1776	12 345, 3104, 1400	4780, 3188, 1991	9834, 6781, 3448	9285, 6162, 2591	13 818, 3489, 2285
Criterion for observed reflections	$I > 2\sigma(I)$	$I > 2\sigma(I)$	$I > 2\sigma(I)$	$I > 2\sigma(I)$	$I > 2\sigma(I)$	$I > 2\sigma(I)$
R_{int}	0.061	0.148	0.050	0.031	0.025	0.047
θ_{max} (°)	25.0	23.3	25.0	26.4	25.0	25.0
Refinement						
Refinement on	F^2	F^2	F^2	F^2	F^2	F^2
$R[F^2 > 2\sigma(F^2)]$, $wR(F^2)$, S	0.048, 0.093, 0.80	0.049, 0.116, 0.77	0.052, 0.163, 0.84	0.050, 0.112, 0.84	0.050, 0.137, 0.82	0.051, 0.137, 1.03
No. of reflections	3634	3103	3188	6781	6162	3489
No. of parameters	259	292	245	419	419	197
H-atom treatment	Mixture of independent and constrained refinement	Mixture of independent and constrained refinement	Constrained to parent site	Constrained to parent site	Constrained to parent site	Constrained to parent site
Weighting scheme	$w = 1/[\sigma^2(F_o^2) + (0.0281P)^2]$, where $P = (F_o^2 + 2F_c^2)/3$	$w = 1/[\sigma^2(F_o^2) + (0.0351P)^2]$, where $P = (F_o^2 + 2F_c^2)/3$	$w = 1/[\sigma^2(F_o^2) + (0.1154P)^2]$, where $P = (F_o^2 + 2F_c^2)/3$	$w = 1/[\sigma^2(F_o^2) + (0.0443P)^2]$, where $P = (F_o^2 + 2F_c^2)/3$	$w = 1/[\sigma^2(F_o^2) + (0.0587P)^2]$, where $P = (F_o^2 + 2F_c^2)/3$	$w = 1/[\sigma^2(F_o^2) + (0.0727P)^2 + 0.0665P]$, where $P = (F_o^2 + 2F_c^2)/3$
$(\Delta/\sigma)_{max}$	0.005	< 0.0001	0.007	< 0.0001	0.001	< 0.0001
$\Delta\rho_{max}$, $\Delta\rho_{min}$ (e Å^{-3})	0.54, −0.57	0.26, −0.17	0.20, −0.15	0.20, −0.16	0.18, −0.09	0.27, −0.17
Extinction method	None	*SHELXTL*	None	None	None	None
Extinction coefficient	–	0.0040 (9)	–	–	–	–

113 electrons in the solvent accessible voids of 591.6 Å^{-3}. This was assigned as 12 water molecules per unit cell, which were added to the formula. The hydroxyl H atom was included in a calculated position so as to form the best hydrogen bond to the hydroxyl group of an adjacent zeaxanthin molecule. The crystal data are summarized in Table 1.[1] All calculations and

[1] Supplementary data for this paper are available from the IUCr electronic archives (Reference: BM5041). Services for accessing these data are described at the back of the journal.

preparation of the plots were carried out using the *SHELXTL* package (Bruker, 2001) and *PLATON* (Spek, 2003).

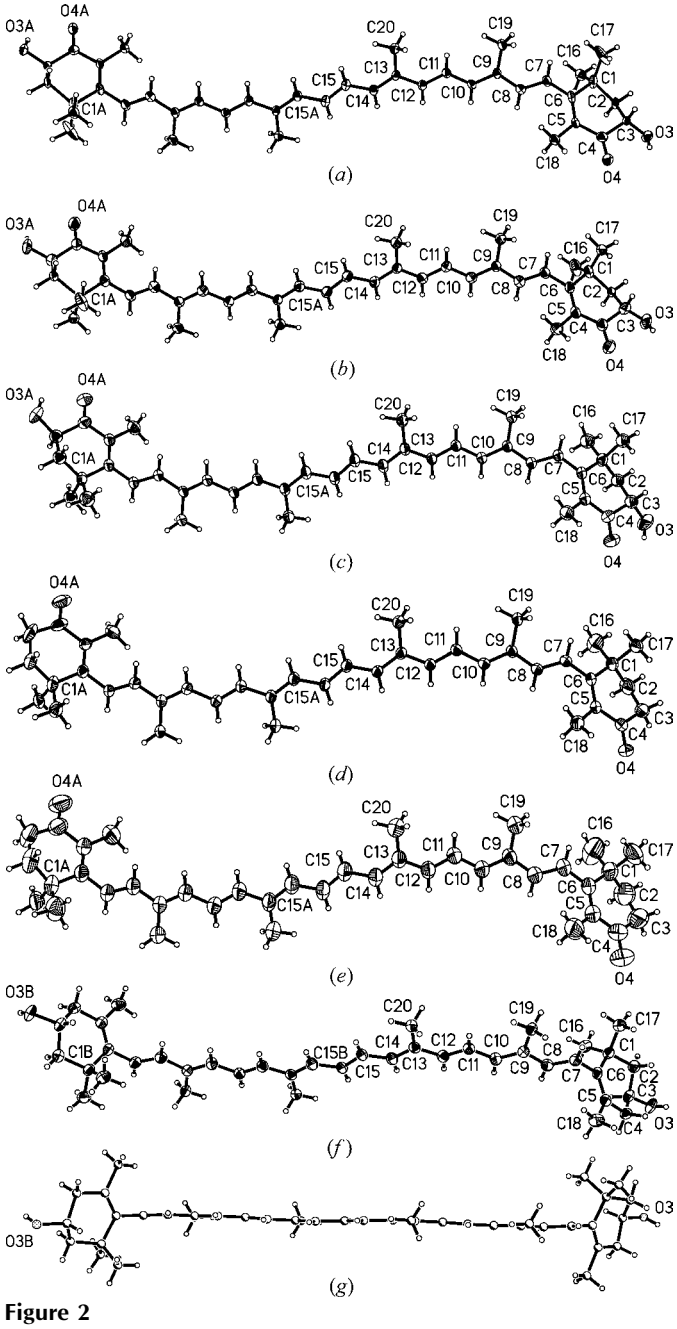

Figure 2
(*a*) Plot of AXT molecule in AXT-Cl, using 50% probability ellipsoids. The chloroform solvate molecule and disordered atoms have been omitted for clarity. (*b*) Plot of AXT molecule in AXT-py, using 50% probability ellipsoids. The pyridine solvate molecule and disordered atoms have been omitted for clarity. (*c*) Plot of AXT molecule in AXT-un at 293 K, using 30% probability ellipsoids; disordered atoms have been omitted for clarity. (*d*) Plot of canthaxanthin at 100 K, using 50% probability ellipsoids; disordered atoms have been omitted for clarity. (*e*) Plot of canthaxanthin at 293 K, using 50% probability ellipsoids; disordered atoms have been omitted for clarity. (*f*) Plot of *RS*-zeaxanthin using 50% probability ellipsoids; disordered water solvent atoms have been omitted. (*g*) Plot of *RS*-zeaxanthin viewed approximately down the plane of the polyene chain, showing that the end rings are twisted out of the plane of the polyene chain [the C5—C6—C7—C8 torsion angle is −74.9 (3)°].

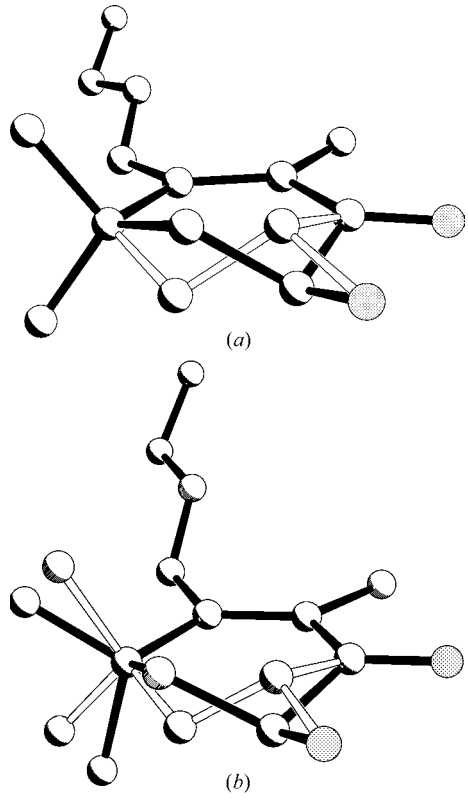

Figure 3
Plot showing the two conformations of the end-rings of (*a*) AXT-Cl at 100 K and (*b*) AXT-un at 293 K.

2.3. UV–vis spectra measurements

UV–vis spectra were measured on a Varian Cary 5000 UV–vis–NIR spectrometer. The solution-state spectra were recorded with the carotenoids dissolved in chloroform. The solid-state spectra were obtained from crystals pressed between two coverslips.

3. Description of the crystal structures

3.1. Comparison of the carotenoid molecules

Plots of the astaxanthins are shown in Figs. 2(*a*)–(*c*). In each case the AXT molecule is centrosymmetric. Disorder is seen in the end rings of the AXT molecules and this disorder is seen even when the space-group symmetry is reduced to the non-centrosymmetric space groups $P1$, $P2_1$ and $P\bar{1}$ for AXT-Cl, AXT-py and AXT-un, respectively. It arises from the fact that the synthetic astaxanthin used was a mixture of *RR*, *SS* and *RS* isomers. The disorder is shown in close up in Figs. 3(*a*) and (*b*) for AXT-Cl and AXT-un, respectively, where in the latter case it was possible to resolve the disorder to include the atoms C16 and C17. For AXT-py, C2, C3 and C16 were likewise found to be disordered. The crystal structures of canthaxanthin at 100 and 293 K are shown in Figs. 2(*d*) and (*e*) where, in contrast to the AXT structures, the asymmetric unit contains the whole molecule. In these structures, the disorder is confined to only

one end ring (atoms C2*A*, C16*A* and C17*A*) and it is clear that the 100 and 293 K structures are very similar to one another, with an r.m.s. deviation between the structures of only 0.05 Å. For zeaxanthin (Figs. 2*f* and *g*) the molecule is centrosymmetric, but this time, because only the (3*R*,3′*S*, *meso*) isomer is present, no disorder of the end-rings is observed.

In all six crystal structures the molecules adopt the 6-s-*cis* conformation. Comparison of the different crystal forms of AXT shows that the corresponding bond lengths and angles of all three structures are normal and within experimental error the same. Fitting of the atoms of the AXT-py and AXT-Cl structures using the program *OFIT* (from the *SHELXTL* package; Bruker, 2001), excluding the disordered atoms, shows that they are very alike, with an r.m.s. deviation of 0.14 Å. The 293 K structure of AXT-un is less similar to AXT-Cl (r.m.s. deviation 0.33 Å), but comparison of the atoms of the polyene chains gives an r.m.s. deviation of 0.1 Å, where the main differences are between the positions of the substituent atoms of the polyene chain, *i.e.* the conformation of the end rings and methyl groups bonded to the polyene chains. In particular, the C5—C6—C7—C8 torsion angle, which shows the degree to which the end rings are twisted out of the plane of the polyene chain are −42.6 (5), −48.9 (5) and −50.4 (3)°, for AXT-Cl, AXT-py and AXT-un, respectively.

The crystal structure of AXT-un is considerably more precise than that determined by Hashimoto *et al.* (2002) with $R_1 = 0.052$ *versus* $R = 0.171$, $wR = 0.131$ in the previous work. Furthermore, the average C—C bond precision in AXT-un is 0.003 Å, whereas Hashimoto *et al.* (2002) measured the carbon–carbon bond lengths to only two decimal places with standard uncertainties of 0.01 or 0.02 Å. Generally the parameters of the two structure determinations agree within experimental error, except in the region of the disordered end ring since the disorder was not modelled in the older study.

The bond lengths and angles of canthaxathin are also very similar to those of the three AXT structures; the r.m.s. deviation of the 100 K structure of canthaxanthin from AXT-Cl is 0.30 Å, that of the polyene chains alone is 0.16 Å and the respective C5—C6—C7—C8 and C5*A*—C6*A*—C7*A*—C8*A* torsion angles are −48.8 (3) and 50.8 (3)° for the 100 K structure and −50.4 (4) and 53.4 (3)° for the 293 K structure. This shows specifically that, in the absence of a crystal structure of AXT at the time of solving the structure of β-CR (Cianci *et al.*, 2002), the model derived from the structure of canthaxanthin (Bart & MacGillavry, 1968) was a reasonable substitute.

Comparison of our results with those of the older study (Bart & MacGillavry, 1968) shows that the geometric parameters are in close agreement, within experimental error; the precision of our results, with the use of modern equipment is as expected, improved; the *R* value in the older study was 0.115, *versus* $R_1 = 0.050$ for both the 100 and 293 K structures reported here. Also the C—C bond length precision ranged from 0.01 to 0.03 Å in the older study, but averaged 0.003 and 0.004 Å for the 100 and 293 K structures reported here, respectively. The r.m.s. deviation of the 293 K structure to the older structure is only 0.03 Å, and of the 100 K structure is

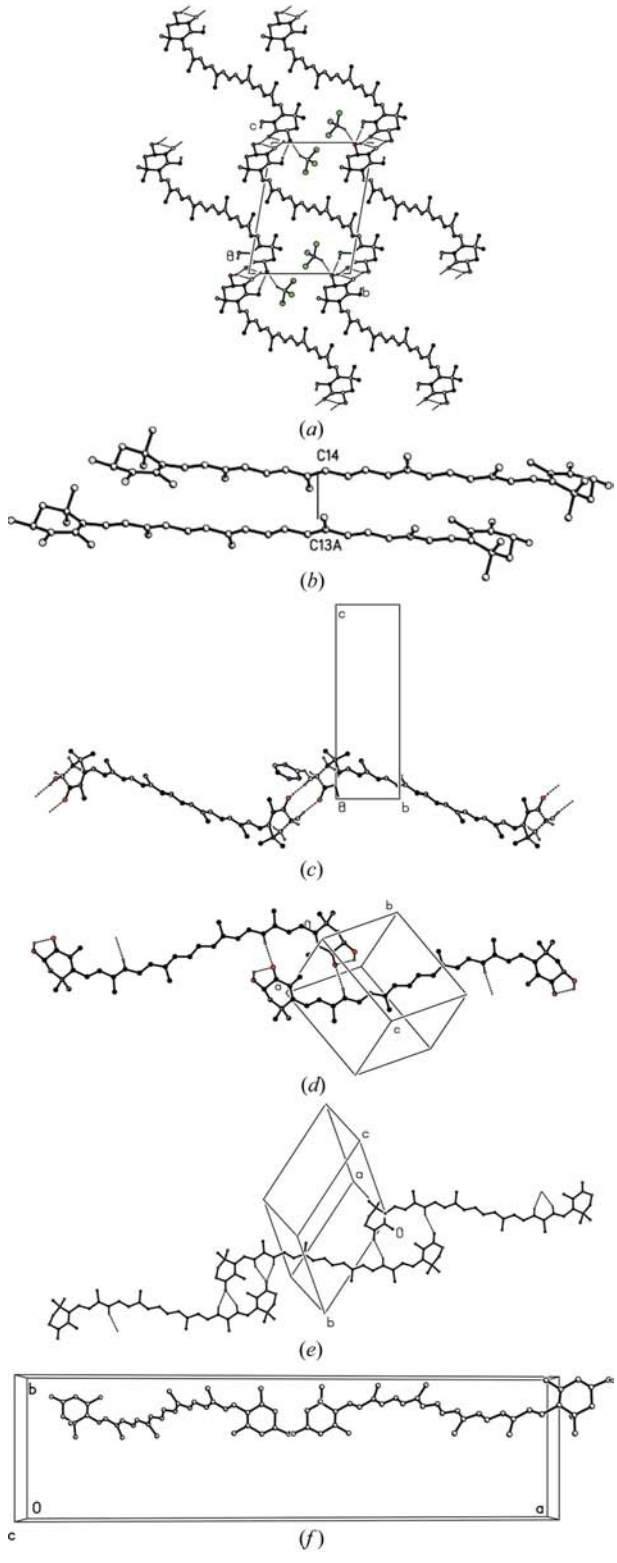

Figure 4
Packing arrangements of the carotenoid crystal structures; disordered atoms and H atoms not involved in hydrogen bonding have been omitted for clarity. (*a*) Packing of AXT-Cl viewed down **a**. (*b*) Plot showing the π-stacking interactions of AXT-Cl. (*c*) Intermolecular hydrogen-bonding interactions of AXT-py viewed down **a**. (*d*). Hydrogen-bonding interactions of AXT-un. (*e*) Intermolecular hydrogen-bonding interactions of canthaxanthin (100 K structure). (*f*) Intermolecular hydrogen-bonding interactions of *RS*-zeaxanthin.

Table 2
Hydrogen bonds for AXT-Cl (Å, °).

D—H···A	$d(D$—H)	d(H···A)	$d(D\cdots A)$	<(DHA)
O3—H3O···O4^{i}	0.834 (17)	2.02 (2)	2.790 (3)	154 (3)
C1S—H1S···O3^{ii}	1.00	2.16	3.061 (4)	150
C18—H18C···O3^{ii}	0.98	2.52	3.460 (4)	161
C18—H18C···O4^{ii}	0.98	2.91	3.557 (4)	124

Symmetry codes: (i) $-x+3, -y, -z+2$; (ii) $-x+2, -y, -z+2$.

Table 3
Hydrogen bonds for AXT-py (Å, °).

D—H···A	$d(D$—H)	d(H···A)	$d(D\cdots A)$	∠(DHA)
O3—H3O···O4^{i}	0.82 (2)	2.03 (3)	2.822 (4)	161 (6)
C4S—H4S···O3	0.95	2.39	3.179 (6)	140

Symmetry codes: (i) $-x+2, -y-1, -z$.

0.06 Å; the latter deviation is similar to that between the new 293 and 100 K structures (0.05 Å).

Comparison of the 100 and 293 K structures indicates that the only significant difference in geometric parameters is in the C5—C6—C7—C8 and C5*A*—C6*A*—C7*A*—C8*A* torsion angles which are −48.8 (3) and 50.8 (3)°, respectively, for the 100 K structure, but significantly larger for the 293 K structure at −50.4 (4) and 53.4 (3)°, respectively, thereby indicating a small temperature dependence. It should also be noted that the largest torsion angle for the three AXT structures is that of the AXT-un measured at 293 K [−50.4 (3)°]; AXT-Cl and AXT-py, both measured at 100 K, had smaller C5—C6—C7—C8 torsion angles of −42.6 (5) and −48.9 (5)°, respectively.

Corresponding bond lengths and angles for *RS*-zeaxanthin, in general, also agree closely with those found for AXT and canthaxanthin. One difference is the C4—C5 bond length which is 1.513 (3) Å for *RS*-zeaxanthin, but ranges from 1.457 (4) to 1.480 (4) Å for the other five structures; however, the C4—C5 bond length in *RS*-zeaxanthin is similar to that in β-carotene, which is 1.500 (7) Å (CSD entry CARTEN2; Allen, 2002) and the bis[menthyl carbonate] derivative of *RR*-zeaxanthin (Linden *et al.*, 2004) at 1.519 (7) and 1.512 (6) Å. This arises from the presence of the keto oxygen at the 4-position in the AXT and canthaxanthin molecules, which leads to a shortening of the C4—C5 bond due to conjugation with the C5—C6 double bond. However, the C4—C5 bond lengths for AXT and canthaxanthin are not as short as the conjugated single bonds of the polyene chains, which range from 1.425 (4) to 1.446 (2) Å for the AXT structures, 1.428 (3) to 1.452 (2) Å for canthaxanthin and 1.427 (3) to 1.449 (3) Å for *RS*-zeaxanthin, with shorter single bonds being found at the centre of the polyene chains. C6—C7 is also longer for *RS*-zeaxanthin at 1.492 (3) Å, than for the three AXT structures where this bond length varies from 1.462 (3) to 1.469 (4) Å, for canthaxanthin where this bond length has values of 1.471 (2) and 1.477 (2) Å and for β-carotene at 1.468 (6) Å (CSD entry CARTEN2; Allen, 2002); for the bis[menthyl carbonate] derivative of *RR*-zeaxanthin (Linden *et al.*, 2004) the C6—C7 distances for the crystallographically different ends are also shorter at 1.473 (7) and 1.468 (7) Å, although the difference is barely significant. In addition, the C5—C6—C7—C8 torsion angle of −74.9 (3)° for *RS*-zeaxanthin (see Fig. 2*g*) is very different to those of AXT and canthaxanthin and also those of β-carotene [−43.1 (7)°, CSD entry CARTEN2; Allen, 2002] and the bis[menthyl carbonate] derivative of *RR*-zeaxanthin [48.4 (8) and 144.5 (6)°; Linden *et al.*, 2004]. The longer C6—C7 bond distance and the C5—C6—C7—C8 torsion angle of −74.9 (3)° indicates that the degree of conjugation of the polyene chain with the end ring for *RS*-zeaxanthin is considerably less than for all the other structures. According to the calculations of Hashimoto *et al.* (2002), this torsion angle for *RS*-zeaxanthin was expected to be 48.7°, and the conformation represented by an angle of −74.9 (3)° was not expected to be stable.

4. Packing of the molecules

4.1. AXT-Cl

A number of different intermolecular interactions determine the packing arrangement in AXT-Cl (Table 2). Firstly, there is pair-wise end-to-end hydrogen bonding between the hydroxyl O atom and the keto O atom; secondly, there is a strong C—H···O hydrogen bond between the chloroform solvent molecule and the hydroxyl O atom, as well as two weaker C—H···O interactions between the H atoms of the C18 methyl group and the hydroxyl and keto O atoms, linking the molecules into chains as shown in Fig. 4(*a*). Finally, the polyene chains pack one above the other at a distance consistent with π-stacking interactions, with a minimum distance of 3.608 (5) Å between C14 and C13 of an adjacent molecule at $-x, -y+1, -z+1$ (Fig. 4*b*).

AXT-py also shows end-to-end pair-wise hydrogen bonding between the hydroxyl and keto O atoms, as well as a weak C—H···O interaction between one C atom of the pyridine solvent molecule and O3, linking the molecules into chains (Table 3, Fig. 4*c*). Again there are π-stacking interactions between the molecules, with a minimum distance of 3.730 (4) Å between C13 and C15($-x, -y-2, -z+1$).

The packing of AXT-un is somewhat different, with an intramolecular hydrogen bond between the hydroxyl and keto oxygen and a weaker C—H···O hydrogen bond linking the molecules into chains (Fig. 4*d*, Table 4). There are also π-stacking interactions, but the molecules are translated with respect to one another compared with the other AXT structures, and the minimum distance between the polyene chains is 3.811 (3) Å between C15 and C9($-x+1, -y+1, -z+1$).

Canthaxanthin, which has no hydroxyl O atoms, has interactions between molecules arising from C—H···O hydrogen bonding (Table 5, Fig. 4*e*). The molecules are also stacked one above the other, indicating π-stacking interactions between the polyene chains, with a minimum distance of 3.482 (3) Å [3.651 (3) Å for the 293 K structure] between C13 and C13($-x, -y+1, -z$). There is a significant difference in both

Table 4
Hydrogen bonds for AXT-un (Å, °).

D—H···A	$d(D$—H)	d(H···A)	$d(D$···$A)$	$\angle(DHA)$
O3—H3···O4	0.84	2.17	2.653 (3)	116
C10—H10···O4^{i}	0.95	2.50	3.439 (3)	168

Symmetry codes: (i) $-x+1, -y, -z$.

Table 5
Hydrogen bonds for canthaxanthin.

D—H···A	$d(D$—H)	d(H···A)	$d(D$···$A)$	$\angle(DHA)$
(*a*) 100 K				
C10—H10···O4^{i}	0.95	2.58	3.438 (2)	150
C10*A*—H10*A*···O4*A*^{ii}	0.95	2.47	3.382 (2)	160
C8*A*—H8*A*···O4*A*^{ii}	0.95	2.57	3.443 (2)	154
(*b*) 293 K				
C10—H10···O4^{i}	0.95	2.60	3.471 (3)	152
C10*A*—H10*A*···O4*A*^{ii}	0.95	2.49	3.412 (3)	163
C8*A*—H8*A*···O4*A*^{ii}	0.95	2.67	3.544 (3)	153

Symmetry codes: (i) $-x-1, -y, -z$; (ii) $-x+2, -y+3, -z+1$.

Table 6
Hydrogen bonds for *RS*-zeaxanthin (Å, °).

D—H···A	$d(D$—H)	d(H···A)	$d(D$···$A)$	$\angle(DHA)$
O3—H3O···O3^{i}	0.82	1.85	2.654 (3)	169

Symmetry codes: (i) $-x+1, y, -z+\frac{5}{2}$.

the intermolecular hydrogen-bonding distances (Table 5) and the π-stacking distances between the 100 and 293 K crystal structures. This is coupled with an anisotropic thermal expansion of the unit-cell dimensions of 1.0% in *a*, 0.7% in *b* and 2.7% in *c*. Although the molecules do not lie along any crystallographic axis, the interactions in the *c* direction are predominantly of van der Waals character, whereas the stronger hydrogen bonding and π-stacking interactions, mainly in the *a* and *b* directions, probably explains the smaller percentage expansion of these axes with temperature.

Finally, for *RS*-zeaxanthin, there are O—H···O hydrogen bonding end-to-end interactions linking the molecules into chains (Table 6, Fig. 4*f*), as well as π-stacking interactions between the polyene chains, with the minimum distance of 3.734 (3) Å between C13 and C15($-x+\frac{1}{2}, -y+\frac{3}{2}, -z$).

5. Discussion

5.1. Comparison of the new carotenoid structures with the AXT molecules in β-CR

The purpose of collecting this ensemble of carotenoid crystal structures was firstly to allow much more precise information to be derived about the geometry and intermolecular interactions of these molecules in the crystal than could be determined from the 3.2 Å resolution protein crystal structure of β-CR (Cianci *et al.*, 2002). Secondly, comparison of the protein bound AXT and these small molecule carotenoid crystal structures may give insight into the bathochromic shift of AXT in the AXT–protein complex.

The first clear difference between the protein-bound AXT molecule and the free carotenoid molecules is that the protein-bound AXT is in the 6-s-*trans* conformation, whereas all the free carotenoids have the 6-s-*cis* conformation. The end rings of the protein-bound AXT molecules are approximately coplanar with the polyene chain, with C5—C6—C7—C8 torsion angles of 172.9 (2) and 177.1 (2)° for each end ring of one of the molecules. In contrast, for the free carotenoid structures, the end rings are twisted out of the plane of the polyene chains by *ca* −43 to −53° for the three AXT structures, for canthaxanthin and for β-carotene; for *RS*-zeaxanthin this torsion angle is −74.9 (3)°, *i.e.* much closer to 90° than for the other carotenoid crystal structures. Comparison of the protein-bound AXT molecule with AXT-Cl using OFIT gives an r.m.s deviation of the two structures of 1.62 Å for the whole molecule and 0.458 Å if only the polyene chains are fitted. Fig. 5(*a*) illustrates the 6-s-*trans* conformation compared with the 6-s-*cis* conformation of AXT-Cl, showing reasonably similar polyene chains, but with the differences in conformation of the end rings clearly illustrated. Fig. 5(*b*) shows the comparison of these two molecules, looking down the plane of the polyene chain, indicating that the end rings of the protein-bound molecule (in blue) are nearly coplanar with the polyene chain, compared with the free AXT-Cl molecule, where the end rings are clearly twisted out of the plane of the polyene chain. In addition it can be seen that the polyene chain of the protein-bound AXT molecule is distinctly bowed compared with that of AXT-Cl. Thus, in the protein-bound molecule of AXT, the polyene chain is fully conjugated with the end ring C5—C6 double bond and the keto oxygen, so that the number of conjugated double bonds is extended to 13. For AXT, canthaxanthin and β-carotene, the conjugation with the end rings is reduced because of the twisting of the end rings out of the plane of the polyene chain; for *RS*-zeaxanthin, there can be little or no conjugation into the end rings due to the −75.9 (3)° C5—C6—C7—C8 torsion angle.

The degree of conjugation into the end rings should in turn affect the colour of the chromophore, with an increase in the length of the conjugated chain leading to a reduced energy gap between the HOMO and LUMO orbitals, resulting in a bathochromic shift (Clayden *et al.*, 2000).

With this in mind, we have measured solution UV–vis spectra, in chloroform, of AXT-Cl, AXT-un, canthaxanthin, *RS*-zeaxanthin and β-carotene, and solid-state spectra for comparison (Figs. 6*a* and *b*). The solution-state spectra show similar peak profiles for AXT and canthaxanthin, with peak maxima at 490 and 482 nm, respectively. The peak profiles of *RS*-zeaxanthin and β-carotene are also similar to one another, showing some structure compared with those of AXT and canthaxanthin, and almost identical absorption maxima of the central peak at 461 and 462 nm, respectively. The difference between the AXT and canthaxanthin peak positions compared with those of *RS*-zeaxanthin and β-carotene reflects the absence of the keto oxygen in the latter carotenoids, reducing

the length of the conjugated polyene chain and therefore leading to an increased energy gap between the HOMO and LUMO orbitals. The peaks in the solid-state spectra were much broader and it was therefore difficult to be certain of the precise positions of the peak maxima. However, AXT-CL AXT-un and canthaxanthin again show very similar peaks at around 480–490 nm, which indicates that there is no significant shift between the chloroform solutions and solid states for these molecules; those of *RS*-zeaxanthin and *β*-carotene are also similar to one another; *RS*-zeaxanthin shows a very broad peak with maxima at 443 and 469 nm, whereas that for *β*-carotene is at 470 nm. Although the broadness of the peaks in these spectra make it difficult to be sure, there is an indication that the spectrum of *RS*-zeaxanthin is shifted to shorter wavelength, which would be in keeping with the much reduced conjugation of the polyene chain into the end ring arising from the −74.9 (3)° C5—C6—C7—C8 torsion angle. The torsion angle for these carotenoids in solution is unknown, but the calculations of Hashimoto *et al.* (2002) suggest that all these molecules, including *RS*-zeaxanthin, should have similar torsion angles of between −40 and −50 °. The similarity of the solution-state spectra of *RS*-zeaxanthin and *β*-carotene suggests that the conformations of these two molecules in solution are probably very similar, but that the packing forces in the crystal have led to a quite different torsion angle for *RS*-zeaxanthin in the solid state. Clearly, improved solid-state spectra are needed and attenuated total reflectance from the surface of an optical waveguide has been effectively exploited previously in order to obtain high-quality UV–NIR absorption spectra of solids (Qi *et al.*, 2002; Ogawa *et al.*, 2004). In addition, such reflectance spectra would provide extinction coefficients of the crystal samples, whereas our method of pressing the crystals between slides does not allow measurement of the sample thickness and so does not provide the extinction coefficient. If we could obtain extinction coefficients of the crystals, we could determine whether hyper- or hypochromic effects accompany the change to the solid state. The available solid-state spectra suggest that the intermolecular hydrogen bonding and *π*-stacking interactions in these crystal structures exert a negligible effect on the positions of the peak maxima. In contrast, the intermolecular interactions of pairs of AXT molecules in the *β*-CR crystal structure with hydrogen bonding of the keto O atom to a bound water at one end and a histidine residue at the other end, their close proximity (minimum distance 7 Å) and their angle of 120° to one another and with the 6-s-*trans* conformation of the molecules lead to the very large bathochromic shift of 100 nm *in vivo*. Further studies on model compounds will vary these parameters in order to determine whether this bathochromic shift can be replicated.

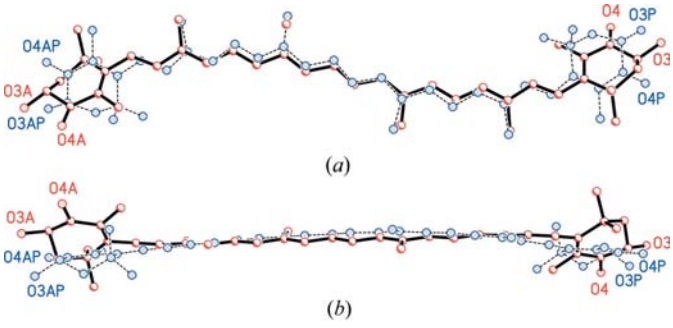

Figure 5
Conformation of AXT-Cl (red) best overlay against the protein-bound AXT (Cianci *et al.*, 2002); (*a*) is the view perpendicular to the plane of the polyene chain and (*b*) is the view edge-on to the polyene chain.

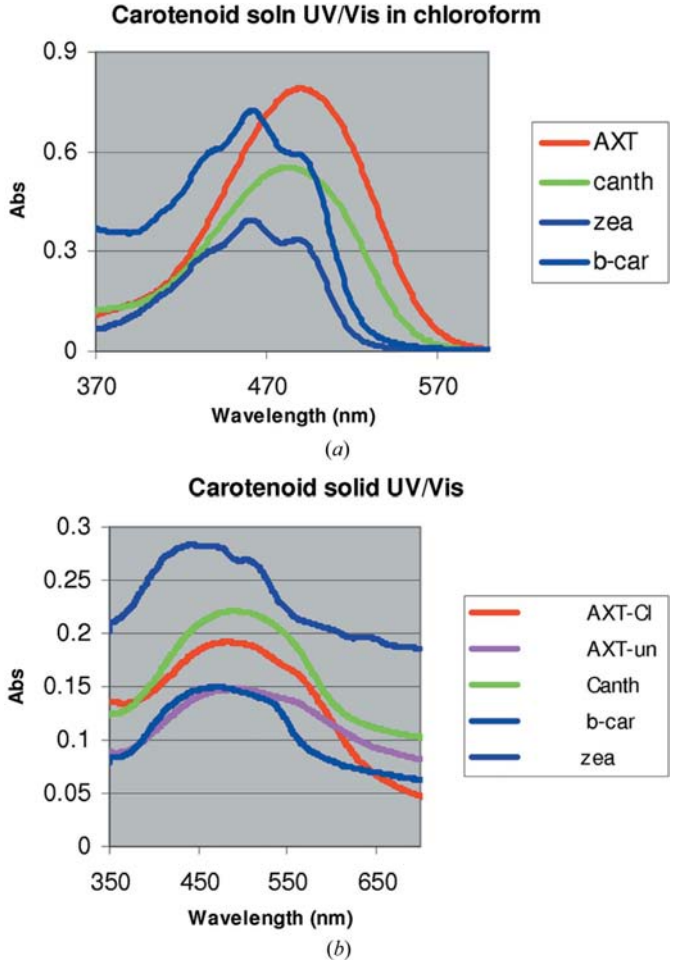

Figure 6
(*a*) Solution-state ($CHCl_3$) UV–vis spectra of AXT, canthaxanthin, *RS*-zeaxanthin and *β*,*β*-carotene. (*b*) Solid-state UV–vis spectra of AXT-Cl, AXT-un, canthaxanthin, *RS*-zeaxanthin and *β*,*β*-carotene.

We thank Dr J. van Thor (University of Oxford), Dr C. I. F. Watt (The University of Manchester) and Dr P. F. Zagalsky (Royal Holloway and Bedford New College) for discussions. We thank EC Marie Curie for a PhD training award (GB) and The Nuffield Foundation for an undergraduate vacation research scholarship (SF).

References

Allen, F. H. (2002). *Acta Cryst.* B**58**, 380–388.
Bart, J. C. J. & Macgillavry, C. H. (1968). *Acta Cryst.* B**24**, 1587–1606.
Bernhard, K. (1989). *Carotenoids: Chemistry and Biology*, edited by N. I. Krinsky, M. M. Mathews-Roth & R. F. Taylor, pp. 337–363. New York: Plenum Press.

Britton G. (1995). *Carotenoids*, Vol. 1B, *Spectroscopy*, edited by G. Britton, S. Liaaen-Jensen & H. Pfander, ch. 2, pp. 43–44. Berlin: Birkhauser Verlag.
Bruker (2001). *SMART*, Version 5.625, *SADABS*, Version 2.03*a,* *SHELXTL*, Version 6.12. Bruker AXS Inc., Madison, Wisconsin, USA.
Bruker (2002). *SAINT*, Version 6.36*a.* Bruker AXS Inc., Madison, Wisconsin, USA.
Chayen, N. E., Cianci, M., Grossmann, J. G., Habash, J., Helliwell, J. R., Nneji, G. A., Raftery, J., Rizkallah, P. J. & Zagalsky, P. F. (2003). *Acta Cryst.* D**59**, 2072–2082.
Cianci, M., Rizkallah, P. J., Olczak, A., Raftery, J., Chayen, N. E., Zagalsky, P. F. & Helliwell, J. R. (2001). *Acta Cryst.* D**57**, 1219–1229.
Cianci, M., Rizkallah, P. J., Olczak, A., Raftery, J., Chayen, N. E., Zagalsky, P. F. & Helliwell, J. R. (2002). *PNAS*, **99**, 9795–9800.
Clayden, J., Greeves, N., Warren, S. & Wothers, P. (2000). *Organic Chemistry.* Oxford University Press.
Cosier, J. & Glazer, A. M. (1986). *J. Appl. Cryst.* **19**, 105–107.
Durbeej, B. & Eriksson, L. A. (2003). *Chem. Phys. Lett.* **375**, 30–38.
Durbeej, B. & Eriksson, L. A. (2004). *PCCP*, **6**, 4190–4198.
Durbeej, B. & Eriksson, L. A. (2006). *PCCP*, **8**, 4053–4071.
Hashimoto, H., Yoda, T., Kobayashi, T. & Young, A. J. (2002). *J. Mol. Struct.* **604**, 125–146.
Ilagan, R. P., Christensen, R. L., Chapp, T. W., Gibson, G. N., Pascher, T., Polivka, T. & Frank, H. A. (2005). *J. Phys. Chem A*, **109**, 3120–3127.
Linden, A., Bürgi, B. & Eugster, C. H. (2004). *Helv. Chim. Acta*, **87**, 1254–1269.
Minichino, A., Habash, J., Raftery, J. & Helliwell, J. R. (2003). *Acta Cryst.* D**59**, 843–849.
Newbiggin, M. I. (1897). *J. Physiol.* **21**, 237–257.
Ogawa, K., Harada, J., Fujiqara, T. & Takahashi, H. (2004). *Chem. Lett.* **33**, 1446.
Qi, Z. M., Matsuda, N., Yoshida, T., Asano, H., Takatsu, A. & Kato, K. (2002). *Optics Lett.* **27**, 2001–2003.
Rønneberg, H., Renstrøm, B., Aareskjold, K., Liaaen-Jensen, S., Vecchi, M., Leuenberger, F. J., Muller, R. K. & Mayer, H. (1980). *Helv. Chim. Acta*, **63**, 711–715.
Renstrøm, B., Rønneberg, H., Borch, G. & Liaaen-Jensen, S. (1982). *Comput. Biochem. Physiol.* **71B**, 253–258.
Rüttimann, A. & Mayer, H. (1980). *Helv. Chim. Acta*, pp. 1456–1480.
Sluis, P. van der & Spek, A. L. (1990). *Acta Cryst.* A**46**, 194–201.
Spek, A. L. (2003). *J. Appl. Cryst.* **36**, 7–13.
Vecchi, M. & Müller, R. K. (1979). *J. High Resolut. Chromatogr. Chromatogr. Commun.* **2**, 195–196.
Wald, G., Nathanson, N., Jencks, W. P. & Tarr, E. (1948). *Biol. Bull.* **95**, 249–250.
Weesie, R. J., Verel, R., Jansen, F. J. H. M., Britton, G., Lugtenburg, J. & deGroot, H. J. M. (1997). *Pure Appl. Chem.* **69**, 2085–2090.
Wijk, A. A. C. van, Spaans, A., Uzunbajakava, N., Otto, C., de Groot, H. J. M., Lugtenburg, J. & Buda, F. (2005). *J. Am. Chem. Soc.* **127**, 1438–1445.
Zagalsky, P. F. (2003). *Acta Cryst.* D**59**, 1529–1531.